This is a preprint, the final version is subject to change, of the American Mineralogist (MSA)
Cite as Authors (Year) Title. American Mineralogist, in press.
DOI: https://doi.org/10.2138/am-2018-6569

Diffusion of molybdenum and tungsten in anhydrous and hydrous granitic melts

Peipei Zhang[1], Li Zhang[1], Zhongping Wang[2], Wan-Cai Li[1,*], Xuan Guo[1], Huaiwei Ni[1,*]

[1] *CAS Key Laboratory of Crust-Mantle Materials and Environments, School of Earth and Space Sciences, University of Science and Technology of China, Hefei 230026, China*

[2] *Physics Experiment Teaching Center, University of Science and Technology of China, Hefei 230026, China*

Corresponding author:

Huaiwei Ni, hwni@ustc.edu.cn

Wan-Cai Li, jifm@ustc.edu.cn

Submitted to American Mineralogist on March 27th, 2018

Revision 1 submitted on August 18th, 2018

This is a preprint, the final version is subject to change, of the American Mineralogist (MSA)
Cite as Authors (Year) Title. American Mineralogist, in press.
DOI: https://doi.org/10.2138/am-2018-6569

ABSTRACT

To better understand the transport of Mo and W in granitic melts and the formation mechanism of porphyry ore deposits, we have investigated the diffusivities of Mo and W in granitic melts with 0.04-5.1 wt% H_2O at 1000-1600 °C and 1 GPa using a diffusion couple approach and a Mo saturation approach with Mo sheet serving as the source. The Mo and W diffusivities obtained from diffusion profiles measured by LA-ICP-MS can be described as:

$$D_{Mo,anhy} = 10^{-1.47\pm0.73}\exp[-(387 \pm 25)/RT],$$

$$D_{W,anhy} = 10^{-1.28\pm1.05}\exp[-(396 \pm 35)/RT],$$

$$D_{Mo,2.7\ wt\%H2O} = 10^{-5.37\pm0.52}\exp[-(211 \pm 18)/RT],$$

$$D_{Mo,5.1\ wt\%H2O} = 10^{-6.87\pm0.69}\exp[-(133 \pm 20)/RT],$$

where D is diffusivity in m^2/s (with the subscripts denoting water contents and "anhy" representing nominally anhydrous melt), R is the gas constant, T is temperature in K, and the activation energies in the exponential are in kJ/mol. When the influence of H_2O is incorporated, Mo diffusivity in granitic melts with <5.1 wt% H_2O can be modeled as:

$$\log D_{Mo} = -(1.94 \pm 1.58) - (0.87 \pm 0.36)w - [(19341 \pm 2784) - (2312 \pm 620)w]/T$$

where w is H_2O content in the melt in wt%. The diffusion behavior (low diffusivities, high activation energies, and strong H_2O effects) of Mo and W indicates that they exist and diffuse in the melt in the form of hexavalent cations. Their low diffusivities imply that the bulk concentrations of Mo and W in exsolved hydrothermal fluid and those in the

melt are probably not in equilibrium. However, because of the large fluid-melt partition coefficients of Mo and W, they can still be enriched, although to a lesser extent than equilibrium partitioning would allow, in the hydrothermal fluid. Slow Mo and W diffusion can be a significant rate-limiting step for the formation of porphyry Mo/W deposits.

Keywords: Porphyry deposits, molybdenum, tungsten, diffusivity, granitic melt

This is a preprint, the final version is subject to change, of the American Mineralogist (MSA)
Cite as Authors (Year) Title. American Mineralogist, in press.
DOI: https://doi.org/10.2138/am-2018-6569

INTRODUCTION

Porphyry-type ore deposits, of which the majority were formed in the Phanerozoic (Kesler and Wilkinson 2008), are commonly found at oceanic or continental arcs above subduction zones (Wilkinson 2013). They are the primary source of copper and molybdenum (approximately accounting for 60% of all mined Cu and 99% of all mined Mo) and an important source of gold, silver and tungsten (Singer 1995; Simon and Ripley 2011). Porphyry deposits are typically large-tonnage and low-grade (e.g., Cu, Mo and W generally less than 1 wt%, 0.2 wt% and 0.2 wt%, respectively; Kirkham and Sinclair 1995). They are associated with intermediate to felsic hypabyssal intrusions (granite porphyry and granodiorite porphyry) located in mid- to shallow crust (Seedorff et al. 2005; Sillitoe 2010).

Porphyry deposits are a cumulative product of a series of geological processes starting from the dehydration of subducted slab (Richards 2005). Within crustal depths, the formation of a porphyry deposit generally involves the following steps (e.g., Annen et al. 2005; Candela and Holland 1986; Candela 1997; Landtwing et al. 2010; Stoffell et al. 2004; Wilkinson 2013): (1) production of metal-containing hydrous magma in the deep crust; (2) emplacement of the magma in the mid- to shallow crust, and enrichment of metals into exsolved magmatic hydrothermal fluid, partly driven by crystallization; (3) deposition of ore minerals locally from the hydrothermal fluid. The second step requires not only that the metals are partitioned into the fluid relative to the silicate melt, but also

that the transport of metals in the melt is rather efficient. Huber et al. (2012) demonstrated with quantitative modeling that rapidly diffusing metals tended to establish equilibrium fluid-melt partition and hence be efficiently scavenged from the melt, whereas slowly diffusing metals would be left behind in the melt. A great deal of effort has been devoted to investigating the partitioning behavior of metals between fluid and melt (e.g., Candela and Holland 1984; Manning and Henderson 1984; Keppler and Wyllie 1991; Bai and Van Groos 1999; Zajacz et al. 2008; Frank et al. 2011; Tattitch and Blundy 2017). By contrast, studies of diffusion kinetics of ore-forming metals in silicate melts are scarce. Among the three major metals of porphyry deposits (Cu, Mo, W; Robb 2004), several recent experimental studies already reported Cu diffusivities (Ni and Zhang 2016; Ni et al. 2017; Ni et al. 2018), but the diffusivity data for W and Mo are much fewer. There was only a single study on W diffusion in anhydrous haplogranitic melt and in that melt doped with extra Na_2O (Mungall et al. 1999). For Mo, there are no measurements to our knowledge.

Due to the lack of Mo and W diffusivity data that are needed for quantitative modeling of processes in the formation of porphyry deposits, the present study experimentally investigates the diffusion of Mo and W in silicate melts of granitic composition. The results are used to discuss the transfer and enrichment of magmatic Mo and W into ore-forming hydrothermal fluids.

This is a preprint, the final version is subject to change, of the American Mineralogist (MSA)
Cite as Authors (Year) Title. American Mineralogist, in press.
DOI: https://doi.org/10.2138/am-2018-6569

EXPERIMENTAL AND ANALYTICAL METHODS

Starting material

The composition of granitic melt was based upon that of the east porphyry of the Chuquicamata porphyry complex, Chile (Ballard 2001), which hosts the largest open pit Cu deposit worldwide. Cu diffusivity in this melt has been reported elsewhere (Ni et al. 2018). Chuquicamata also produces a significant amount of molybdenum (Ossandon et al., 2001).

The anhydrous granitic glass Anhy-Gran was synthesized by fusing a mixture of oxides (SiO_2, Al_2O_3, MgO, Fe_2O_3, TiO_2) and carbonates (K_2CO_3, Na_2CO_3, $CaCO_3$) at 1600 °C in a muffle furnace for 4 h, after decarbonation at 1000 °C for 10 h. Then glass powder of Anhy-Gran was divided into three parts. Two parts were doped with different amounts of MoO_3 and WO_3 and remelted at 1600 °C for 4 h to obtain Mo-rich, W-poor (Anhy-Gran-Mo) and W-rich, Mo-poor (Anhy-Gran-W) granitic glasses. The doped glasses were crushed and remelted at 1600 °C for 4 h to ensure homogeneous distribution of Mo and W. Electron microprobe analyses show that the major compositions of the synthesized glasses closely resembled the east Chuquicamata porphyry (Table 1). LA-ICP-MS analyses indicate that Mo and W were distributed homogeneously in the Mo and W doped glasses. Anhy-Gran-Mo contains ~1900 ppm and ~300 ppm of Mo and W, respectively. Anhy-Gran-W contains ~1900 ppm and ~300 ppm W and Mo, respectively (Table 1). Water contents of these glasses were found to be ~110 ppm based upon FTIR

measurements. To synthesize hydrous granitic glasses, the mixture of anhydrous glass powder and distilled water was sealed in a Pt capsule and fused at 1200 °C and 0.5 GPa in a piston cylinder apparatus for 12 h. The hydrous glasses synthesized from the third part of Anhy-Gran (undoped with Mo or W) contained ~2.8 wt% or ~5.1 wt% H_2O, whereas those synthesized from Anhy-Gran-Mo and Anhy-Gran-W contained ~3.9 wt% H_2O. All of the synthesized glasses had a light brown color and were free of crystals. The anhydrous glasses contained a small amount of air bubbles.

Diffusion experiments

The diffusion experiments were carried out in a 3/4" end-loaded piston cylinder apparatus at the University of Science and Technology of China (USTC). Two different approaches were adopted. The diffusion couple approach, aimed at obtaining Mo and W diffusivities together, involved two halves, with one being Mo-rich and W-poor and the other being W-rich and Mo-poor. Two granitic glass cylinders with a diameter of 2.7 mm and a height of 1.5 mm were doubly polished and welded shut in a Pt capsule of 3 mm outer diameter and 0.15 mm wall thickness, with the W-rich half being placed at bottom (Fig. 1a). In Mo-saturated diffusion experiments aimed at obtaining Mo diffusivity, an undoped granitic glass cylinder of 1.5-2.5 mm height and 2.7 mm (for the samples with ~2.9 wt% H_2O) or 4.7 mm (for the samples with ~5.1 wt% H_2O) diameter was placed on top of a Mo sheet of 25 μm thickness, with the latter serving as the source of Mo (Fig.

129 1b). They were welded shut in a Pt capsule of 3 mm or 5 mm outer diameter and 0.15
130 mm wall thickness.

131 From the outside to the inside, the sample assembly comprised of talc, Pyrex glass,
132 graphite heater and crushable MgO with the Pt capsule fit inside. A type-S thermocouple
133 at the top of the Pt capsule served to monitor the temperature during the experiment. The
134 thermocouple tip was only ~2 mm away from the portion of the sample containing the
135 effective diffusion profile. The thermal gradient over that distance was found to be small,
136 and therefore no temperature correction was applied. A piston-out procedure was used
137 and a pressure correction of 15% was applied (Guo et al. 2016). The sample assembly
138 was first relaxed at 473 K and 1 GPa for at least 2 hours and was then rapidly heated (at
139 100 °C/s) to the target temperature ranging from 1000-1600 °C by a programmed
140 procedure. The 1 GPa pressure guaranteed that the hydrous melts remained to be water
141 undersaturated. Rapid quench by turning off the power was applied after a dwell time of
142 1-93 h to achieve appropriate diffusion distances.

143 After the diffusion experiments, the recovered samples were cut into two halves
144 longitudinally using a diamond saw. One half was mounted into epoxy resin and polished
145 for LA-ICP-MS analysis of Mo and W concentrations, and the other half was doubly
146 polished for FTIR analysis to measure H_2O contents.

147

148 **Analytical methods**

149 The major element compositions of the granitic glasses were analyzed with a
150 Shimadzu EPMA-1600 electron microprobe at USTC using a beam of 15 kV, 10 nA and
151 10 μm diameter. Twelve points were measured on each glass to obtain an average
152 composition.

153 Water contents of the starting glass cylinders and the experimental products were
154 measured by a Spotlight 200 microscope system attached to a PerkinElmer Frontier FTIR
155 spectrometer at USTC, using an MIR or NIR source, a CaF_2 or KBr beamsplitter, and an
156 MCT detector. FTIR spectra were collected using 64 scans. Multiple measurements
157 confirmed that water was homogeneously distributed in the samples. For the nominally
158 anhydrous glasses, the calibration of Leschik et al. (2004) for the O-H stretching band at
159 3550 cm^{-1} (a linear molar absorptivity of 8.0 L mol^{-1} mm^{-1}) was used. For the hydrous
160 glasses, the calibration of Withers and Behrens (1999) for the combination bands at 5200
161 cm^{-1} (0.166 L mol^{-1} mm^{-1}) and 4500 cm^{-1} (0.141 L mol^{-1} mm^{-1}) was used to obtain
162 molecular H_2O and OH concentrations, where the baselines were fit by two tangential
163 lines (TT calibration). The total water contents were obtained by summing the
164 concentrations of the two hydrous species.

165 Concentrations of Mo and W of granitic glasses before and after diffusion
166 experiments were measured with LA-ICP-MS at USTC (Coherent GeoLas HD Excite
167 excimer 193nm short pulse width attached to Agilent 7900 quadrupole mass
168 spectrometer). The sample chamber was flushed with helium at a rate of 0.5 L/min, with

169 1 L/min Ar being added on the way to the ICP-MS. Spot analyses were performed with a
170 beam diameter of 32 μm and repetition rate of 6 Hz. For each analysis, the sample was
171 measured for 45 s (7 ms dwell time for each mass) after measurement of the gas
172 background for 20 s. The analytical results were processed with the ICPMSDataCal
173 routine (Liu et al. 2008; Chen et al. 2011). External standardization was performed on the
174 NIST SRM 610 and SRM 612 silicate glass (used for Mo and W), BCR-2G, BHVO-2G
175 and BIR-1G. Internal standardization was achieved by normalizing the total of all of the
176 measured elements to 100%. Detection limits were of the order of 1 ppm, and typical
177 analytical precision was 2% to 4%. For each experimental product, 3 diffusion profiles
178 consisting of 30-80 points were measured along the centerline and 250 μm apart from it
179 on both sides (Fig. 2).
180

181 **RESULTS**

182 Four diffusion couple experiments and nine Mo saturation experiments have been
183 conducted, with the conditions and results presented in Table 2. The recovered samples
184 have largely preserved their original geometry (Figure 2). Although the samples usually
185 contained several cracks quasi-perpendicular to the cylindrical axis, diffusion profiles
186 across the cracks appeared to be smooth. As such, we decided not to correct for the
187 widths of cracks, which are much shorter than the diffusion profiles.

188 LA-ICP-MS analyses indicate that the major element compositions of experimental

189 products remain essentially unchanged except for FeO. For the samples from diffusion
190 couple experiments, FeO contents adjacent to capsule walls dropped to 0.5-1.2 wt%, due
191 to the widely known problem of Fe loss to Pt (Holloway and Wood 1988), but this did
192 not affect melt interior where Mo and W diffusion profiles reside. The samples from Mo
193 saturation experiments suffered more severe Fe loss. In most of them, FeO contents
194 decreased from 0.5-1.0 wt% at the Mo end to 0.04-0.2 wt% at the opposite end,
195 indicating a weaker affinity of Fe with Mo than with Pt. One exception is sample
196 Hydr-Gran-9, with FeO content being lower (~0.5 wt%) at the Mo end and higher (~1.0
197 wt%) at the opposite end.

198 FTIR analyses show that the anhydrous samples have gained a small amount of water
199 after experiments, with H_2O content increased to 0.06-0.19 wt% (Table 2). Most hydrous
200 samples have preserved their original water (Table 2). However, the H_2O content of
201 Hydr-Gran-4 decreased from 3.0 to 2.3 wt%. More severe water loss was found for
202 Hydr-Gran-9, the H_2O content of which dropped from 5.1 wt% to 3.6 wt%. To keep
203 consistency, the mean value of initial and final water contents was used to characterize
204 the sample regardless of the degree of water loss or gain (Table 2).

205

206 **Fitting of diffusion profiles**

207 The Mo and W concentration profiles measured along the centerlines of samples
208 were used for fitting and extraction of diffusivity. Those from diffusion couple

experiments (Fig. 3) were fit by the analytical solution for one-dimensional diffusion in an infinite medium (Crank 1975):

$$C = \frac{C_{+\infty} + C_{-\infty}}{2} + \frac{C_{+\infty} - C_{-\infty}}{2} erf \frac{x - x_0}{\sqrt{4Dt}}, \quad (1)$$

where $C_{+\infty}$ and $C_{-\infty}$ are the initial concentrations of Mo or W of the two halves of the diffusion couple respectively, x_0 is the position of the interface, t is time, and D is diffusivity of Mo or W. Given that the locus of the original interface cannot be determined precisely, x_0 is not constrained in fitting.

The concentration profiles of Mo saturation experiments (Fig. 4) were fit by the analytical solution for one-dimensional diffusion in semi-infinite medium (Crank 1975):

$$C = C_0 + (C_\infty - C_0) erf \frac{x}{\sqrt{4Dt}}, \quad (2)$$

where C_∞ is the initial Mo concentration of the undoped granitic glass and is taken to be zero, and C_0 is the Mo concentration at the melt-Mo interface (i.e., Mo solubility) and is not constrained.

The values of C_0 from fitting are summarized in Table 2, ranging from 0.25 wt% to 1.8 wt%. Interface Mo concentration increases with increasing temperature and H_2O content (Fig. 5). However, Hydr-Gran-9, the sample that experienced the most significant water loss, shows abnormally high C_0 at 1000 °C which is inconsistent with the general trend.

228 **Diffusivities of Mo and W in granitic melts**

229 The diffusivities of Mo and W obtained from least-squares regression of measured
230 profiles with error function curves (equation 1 and equation 2) are summarized in Table 2
231 and Figure 6. Results from the four diffusion couple experiments indicate similar
232 diffusivity for Mo and W at both anhydrous and hydrous conditions. In addition, the two
233 experimental approaches, diffusion couple and Mo saturation, yield consistent diffusivity
234 values.

235 The data sets collected at a series of temperatures but roughly the same H_2O content
236 show good agreement with the Arrhenius relationship $D = D_0\exp(-E_a/RT)$ with D_0 being
237 the pre-exponential factor, E_a being the activation energy, R being the gas constant, and T
238 being temperature. Diffusivities of Mo and W in nominally anhydrous granitic melt (with
239 H_2O <0.1 wt%) at 1 GPa and 1400-1600 °C can be expressed by the following Arrhenius
240 relations:

241 $$D_{Mo,anhy} = 10^{-1.47\pm0.73}\exp[-(387\pm25)\text{kJ/mol}/RT] \quad (3)$$

242 $$D_{W,anhy} = 10^{-1.28\pm1.05}\exp[-(396\pm35)\text{kJ/mol}/RT] \quad (4)$$

243 where D is in m^2/s and T is in K.

244 Diffusivities of Mo in hydrous granitic melts with ~2.7 wt% and ~5.1 wt% H_2O at 1
245 GPa and 1400-1600 °C and 1100-1400 °C can be expressed by the following expressions,
246 respectively:

247 $$D_{Mo,2.7wt\%H2O} = 10^{-5.37\pm0.52}\exp[-(211\pm18)\text{kJ/mol}/RT] \quad (5)$$

This is a preprint, the final version is subject to change, of the American Mineralogist (MSA)
Cite as Authors (Year) Title. American Mineralogist, in press.
DOI: https://doi.org/10.2138/am-2018-6569

$$D_{Mo,5.1\ wt\%H2O} = 10^{-6.87\pm0.69}\exp[-(133\pm20)kJ/mol/RT] \quad (6)$$

where D is in m^2/s and T is in K.

Water has a significant impact on Mo and W diffusion in granitic melt. Using nominally anhydrous melt as the benchmark, at 1400 °C, Mo diffusivity increases by a factor of 40 with the addition of 2.7 wt% H_2O, and by a factor of 300 with 5.1 wt% H_2O. If extrapolated to 800 °C, a more realistic temperature for felsic magmatic systems, the influence of water would be much more dramatic: Mo diffusivity would increase by 7 orders of magnitude with the addition of 5.1 wt% H_2O. The strong influence of water is also evident with regard to activation energy: E_a for Mo diffusion decreases from 387 kJ/mol in anhydrous granitic melt to 211 kJ/mol at 2.7 wt% H_2O, and to 133 kJ/mol at 5.1 wt% H_2O. When compared to the diffusivities of other cations (e.g., Mungall et al. 1999), the influence of water on Mo and W is stronger than that on rapidly diffusing species such as Ca and Sr, but is weaker than that on slowly diffusing species such as Zr and Hf.

The logarithm of Mo diffusivity at 1400 °C increases roughly linearly with H_2O content (Fig. 7a). Closer inspection reveals that both the logarithm of the pre-exponential factor D_0 (Fig. 7b) and the activation energy E_a (Fig. 7c) decrease roughly linearly with H_2O content. Based on the data sets of Mo diffusivity at three different H_2O contents (<0.1 wt%, ~2.7 wt%, and ~5.1 wt%), the following general expression of Mo diffusivity at 1 GPa in granitic melts containing <5.1 wt% H_2O was obtained:

$$\log D_{Mo} = -(1.94 \pm 1.58) - (0.87 \pm 0.36)w - [(19341 \pm 2784) - (2312 \pm 620)w]/T \quad (7)$$

where D is in m^2/s, w is water content in granitic melt in wt%, and T is in K. Equation (7) reproduces the majority of log$D$ values to within 0.16 log$D$ units. When the mean values of initial and final H_2O contents are used, the Mo diffusivity data obtained from Hydr-Gran-1 and Hydr-Gran-9 are roughly consistent with equation (7), despite that these data were not used for developing the general expression and that Hydr-Gran-9 experienced severe H_2O loss and has an abnormally high interface Mo concentration. In view of the similarity between W diffusivity and Mo diffusivity, equation (7) is also considered to be applicable to describing W diffusion.

DISCUSSION AND IMPLICATIONS

Complications

One may question whether convection has shaped the measured Mo and W concentration profiles in granitic melts. In their study on Cu diffusion, Ni et al. (2017) dismissed a significant convection effect based upon three lines of reasoning: (1) granitic melts have high viscosity; (2) multiple traverses give consistent diffusion profiles; (3) experiments with different dwell durations yield consistent diffusivity. These arguments are also applicable to our experiments. For example, three traverses, one along the centerline and the other two 250 μm apart from it on each side (Fig. 2), show good consistency (Fig. 3 and Fig. 4). The regular variation of diffusivity with temperature and

288 H_2O content also imply that convection was unlikely a serious problem in our
289 experiments.

290 At the effective diffusion profiles, the limited changes in FeO contents (negligible in
291 diffusion couple experiments but from 1.7 wt% to 0.5-1.0 wt% in Mo saturation
292 experiments) are not expected to have any major effect on Mo and W diffusion. Sample
293 Hydr-Gran-9 shows severe H_2O loss (5.1 wt% dropped to 3.6 wt%), abnormally high
294 interface Mo concentration (1.8 wt%), and atypical Fe-loss pattern (more severe at the
295 Mo end than at the opposite Pt end). H_2O loss was probably due to failure of the Pt
296 capsule during the long dwell duration (43 h). We infer that H_2O escaped from the melt
297 in the form of H_2, leaving behind an increased Fe^{3+}/Fe^{2+} ratio and hence increased
298 intrinsic oxygen fugacity. A more oxidized environment would mitigate Fe loss to Pt
299 (Ford 1978). On the other hand, it probably enhanced the dissolution of Mo into the melt,
300 giving rise to an abnormally high C_0. To be on the safe side, we excluded this experiment
301 when developing the general expression of Mo diffusivity, but the Mo diffusivity
302 obtained from Hydr-Gran-9 appears to be roughly consistent with equation (7) when the
303 mean value of the initial and final water contents is used for calculation.

304 Oxygen fugacity was not controlled in our experiments. The intrinsic redox state of
305 our sample assembly was probably close to the fayalite-magnetite-quartz (FMQ) buffer
306 (Jakobsson 1997), but the starting anhydrous granitic melts were more oxidized because
307 they were synthesized in air. The speciation of Mo and W in silicate melts is not sensitive

to redox state: these two elements exist predominantly as Mo^{6+} and W^{6+} in silicate glasses and melts over a broad range of oxygen fugacity, from air to the iron-wüstite buffer (Farges et al. 2006a, 2006b; O'Neill et al. 2008; Wade et al. 2013). Therefore, the diffusion of Mo and W is unlikely to be affected by oxygen fugacity in a significant way.

One may also wonder whether the similar Mo and W diffusivities obtained from diffusion couple experiments were an artifact of interdiffusion. In other words, Mo diffusion and W diffusion were coupled and what was measured is actually Mo-W interdiffusivity. However, Mo and W are generally trace, or at most minor, elements in the melts, since even the interface Mo concentrations are typically only several thousand ppm (Table 2). In Mo saturation experiments, despite the decrease of Mo activity from ~1 at the interface to ~0 at far interior of the melt, the diffusion profiles can be well fit by error function curves, indicating trace element behavior of Mo. Furthermore, in both anhydrous and hydrous melts, the Mo diffusivities obtained from diffusion couple experiments are in good agreement with those from Mo saturation experiments. We therefore conclude that Mo and W behave as trace elements in silicate melts and should not interfere much with each other with respect to diffusion. The similarity between Mo diffusivity and W diffusivity is real.

Comparison with previous work

Mungall et al. (1999) measured diffusivities of W alongside other 17 trace elements

328 in anhydrous haplogranitic melt containing 80 wt% SiO_2 and 12% Al_2O_3, at 1600, 1400,
329 1137 °C and 1 atm. Compared to their composition, our granitic melt is less siliceous and
330 more aluminous. Considering that the pressure effect for element diffusion in silicate
331 melt is generally negative and is less significant compared to the influence of
332 temperature and H_2O content (Zhang et al. 2010), the small difference in W diffusivity
333 between Mungall et al. (1999) and this study (Fig. 8) is attributed mainly to the
334 difference in melt composition rather than to the 1 GPa pressure gap. The W diffusivity
335 data in haplogranitic melt doped with 20 wt% Na_2O are comparable to Mo diffusivity in
336 granitic melt with 5 wt% H_2O, indicating a stronger influence of H_2O than Na_2O on a
337 wt% basis (but comparable on a molar basis).

338 In anhydrous granitic melts, diffusivities of W and Mo are much lower than those of
339 univalent and divalent cations such as Cu^+ and Ca^+, but are similar to those of
340 pentavalent cations such as Nb^{5+} and Ta^{5+} (Fig. 8). This is consistent with that Mo and W
341 exist and diffuse in the form of hexavalent cations in silicate melts, since Mo^{6+}, W^{6+},
342 Nb^{5+} and Ta^{5+} not only are similar with respect to valence but also have almost identical
343 ionic radii (0.073-0.078 nm, Shannon 1976) in octahedral sites.

344

345 **Implications**

346 Compared to porphyry Cu deposits, porphyry Mo deposits and porphyry W deposits
347 generally formed at greater depths, at a minimum of 4-8 km (Simon and Ripley 2011;

Robb 2004). In the formation of porphyry Mo and W deposits, before reaching the point of water saturation, a significant degree of crystallization probably took place. As Mo and W are incompatible elements, crystallization tended to enrich Mo and W in silicate melt (Robb 2004; Adam and Green 2006, 2011; Wilkinson 2013), unless a sulfide phase formed which strongly sequestered Mo (Mengason et al. 2011; Li and Audétat 2012).

For the growth of hydrothermal fluid bubbles from silicate melt, H_2O is the principal equilibrium-determining component as defined in Zhang (2008). In a hydrous granitic melt with ~5 wt% H_2O, Mo diffusivity at 800 °C is estimated to be 2 orders of magnitude lower than H_2O diffusivity (Ni and Zhang 2008; Fig. 8). Therefore, the concentrations of Mo and W in the fluid are unlikely in equilibrium with their bulk concentrations in the melt. The degree of disequilibrium is also controlled by their partitioning behavior. The fluid-melt partition coefficients (K) of Mo and W increase with the salinity of the fluid and mostly fall in the range of 5 to 100 (Manning and Henderson, 1984; Zajacz et al., 2008; Tattitch and Blundy 2017 and references therein). According to equation (4-145) in Zhang (2008), the enrichment factor (the ratio of element concentration in the fluid over that in the melt) of a trace element can be estimated by

$$EF = \frac{K}{1+\sqrt{\pi}\gamma e^{\gamma^2}\left[1-erf(\gamma)\right](K-1)}, \qquad (8)$$

where γ is a dimensionless factor proportional to the square root of the diffusivity ratio D/D_{H2O}. When $D << D_{H2O}$, $\gamma >> 1$ and $\sqrt{\pi}\gamma e^{\gamma^2}\left[1-erf(\gamma)\right] \approx 1$, leading to an enrichment factor of 1. In this limiting case, the hydrothermal fluid will have the same concentration

as the bulk melt (i.e., no enrichment). For Mo and W, the difference between their diffusivity and D_{H2O} may result in γ in the range of 0.1 to 2, leading to enrichment factors smaller than K but larger than 1 (Fig. 9).

In summary, owing to the large partition coefficients of Mo and W between fluid and melt, they can still be enriched, although to a lesser extent than equilibrium partitioning would allow, in the hydrothermal fluid. However, the slow diffusive transport of Mo and W in silicate melts can be a significant rate-limiting step for the formation of porphyry deposits.

ACKNOWLEDGEMENTS

We thank Ting Liang for assistance in LA-ICP-MS analyses. This study was supported by the National Natural Science Foundation of China (41602030, 41590622, 41721002), China Postdoctoral Science Foundation (2016M592058), the 111 Project of Ministry of Education, China, and the Fundamental Research Funds for the Central Universities of China (WK2080000102).

REFERENCES CITED

Adam, J., and Green, T. (2006) Trace element partitioning between mica-and amphibole-bearing garnet lherzolite and hydrous basanitic melt: 1. Experimental results and the investigation of controls on partitioning behaviour. Contributions to

388 Mineralogy and Petrology, 152, 1-17.

389 Adam, J., and Green, T. (2011) Trace element partitioning between mica-and
390 amphibole-bearing garnet lherzolite and hydrous basanitic melt: 2. Tasmanian
391 Cainozoic basalts and the origins of intraplate basaltic magmas. Contributions to
392 Mineralogy and Petrology, 161(6), 883-899.

393 Annen, C., Blundy, J.D., and Sparks, R.S.J. (2005) The genesis of intermediate and
394 silicic magmas in deep crustal hot zones. Journal of Petrology, 47, 505-539.

395 Bai, T.B., and Van Groos, A.K. (1999) The distribution of Na, K, Rb, Sr, Al, Ge, Cu, W,
396 Mo, La, and Ce between granitic melts and coexisting aqueous fluids. Geochimica
397 et Cosmochimica Acta, 63, 1117-1131.

398 Ballard, J.R. (2001) A comparative study between the geochemistry of ore-bearing and
399 barren calc-alkaline intrusions, 193 p. Ph.D. thesis, The Australian National
400 University, Canberra.

401 Candela, P.A. (1997) A review of shallow, ore-related granites: textures, volatiles, and ore
402 metals. Journal of petrology, 38, 1619-1633.

403 Candela, P.A., and Holland, H.D. (1984) The partitioning of copper and molybdenum
404 between silicate melts and aqueous fluids. Geochimica et Cosmochimica Acta, 48,
405 373-380.

406 Candela, P.A., and Holland, H.D. (1986) A mass transfer model for copper and
407 molybdenum in magmatic hydrothermal systems; the origin of porphyry-type ore

deposits. Economic Geology, 81, 1-19.

Chen, L., Liu, Y.S., Hu, Z.C., Gao, S., Zong, K.Q., and Chen, H.H. (2011) Accurate determinations of fifty-four major and trace elements in carbonate by LA-ICP-MS using normalization strategy of bulk components as 100%. Chemical Geology, 284, 283-295.

Crank, J. (1975) The Mathematics of Diffusion, 414 p. Clarendon, Oxford.

Farges, F., Siewert, R., Brown, G.E. Jr., Guesdon, A., and Morin, G. (2006a) Structural environments around molybdenum in silicate glasses and melts. I. Influence of composition and oxygen fugacity on the local structure of molybdenum. The Canadian Mineralogist, 44, 731-753.

Farges, F., Siewert, R., Ponader, C.W., Brown, G.E. Jr., Pichavant, M., and Behrens, H. (2006b) Structural environments around molybdenum in silicate glasses and melts. II. Effect of temperature, pressure, H_2O, halogens and sulfur. The Canadian Mineralogist, 44, 755-773.

Ford, C.E. (1978) Platinum-iron alloy sample containers for melting experiments on iron-bearing rocks, minerals, and related systems. Mineralogical Magazine, 42(322), 271-275.

Frank, M.R., Simon, A.C., Pettke, T., Candela, P.A., and Piccoli, P.M. (2011) Gold and copper partitioning in magmatic-hydrothermal systems at 800 °C and 100 MPa. Geochimica et Cosmochimica Acta, 75, 2470-2482.

Guo, X., Zhang, L., Behrens, H., and Ni, H. (2016) Probing the status of felsic magma reservoirs: Constraints from the *P*–*T*–H_2O dependences of electrical conductivity of rhyolitic melt. Earth and Planetary Science Letters, 433, 54-62.

Holloway, J.R., and Wood, B.J. (1988) Simulating the Earth: experimental geochemistry, 208 p. Springer Science, Business Media, Berlin.

Huber, C., Bachmann, O., Vigneresse, J.L., Dufek, J., and Parmigiani, A. (2012) A physical model for metal extraction and transport in shallow magmatic systems. Geochemistry, Geophysics, Geosystems, 13, Q08003.

Jakobsson, S. (1997) Solubility of water and carbon dioxide in an icelandite at 1400 °C and 10 kilobars. Contributions to Mineralogy and Petrology, 127, 129-135.

Keppler, H., and Wyllie, P.J. (1991) Partitioning of Cu, Sn, Mo, W, U, and Th between melt and aqueous fluid in the systems haplogranite-H_2O-HCl and haplogranite-H_2O-HF. Contributions to Mineralogy and Petrology, 109, 139-150.

Kesler, S.E., and Wilkinson, B.H. (2008) Earth's copper resources estimated from tectonic diffusion of porphyry copper deposits. Geology, 36, 255-258.

Kirkham, R.V. and Sinclair W.D. (1995) Porphyry copper, gold, molybdenum, tungsten, tin, silver. In O.R. Eckstrand, W.D. Sinclair and R.I. Thorpe, Ed., Geology of Canadian mineral deposit types, No. 8, p. 421-446. Geological Society of America, New York.

Landtwing, M.R., Furrer, C., Redmond, P.B., Pettke, T., Guillong, M., and Heinrich, C.A.

(2010) The Bingham Canyon porphyry Cu-Mo-Au deposit. III. Zoned copper-gold ore deposition by magmatic vapor expansion. Economic Geology, 105, 91-118.

Leschik, M., Heide, G., Frischat, G.H., Behrens, H., Wiedenbeck, M., Wagner, N., Heide, K., Geißler, H., Reinholz, U. (2004) Determination of H_2O and D_2O contents in rhyolitic glasses. Physics and Chemistry of Glasses, 45, 238-251.

Li, Y., and Audétat, A. (2012) Partitioning of V, Mn, Co, Ni, Cu, Zn, As, Mo, Ag, Sn, Sb, W, Au, Pb, and Bi between sulfide phases and hydrous basanite melt at upper mantle conditions. Earth and Planetary Science Letters, 355, 327-340.

Liu Y.S., Hu Z.C., Gao S., Günther D., Xu J., Gao C.G., and Chen H.H. (2008) In situ analysis of major and trace elements of anhydrous minerals by LA-ICP-MS without applying an internal standard. Chemical Geology, 257, 34-43.

Manning, D.A., and Henderson, P. (1984) The behaviour of tungsten in granitic melt-vapour systems. Contributions to Mineralogy and Petrology, 86, 286-293.

Mengason, M.J., Candela, P.A., and Piccoli, P.M. (2011) Molybdenum, tungsten and manganese partitioning in the system pyrrhotite–Fe–S–O melt–rhyolite melt: impact of sulfide segregation on arc magma evolution. Geochimica et Cosmochimica Acta, 75(22), 7018-7030.

Mungall, J.E., Dingwell, D.B., and Chaussidon, M. (1999) Chemical diffusivities of 18 trace elements in granitoid melts. Geochimica et Cosmochimica Acta, 63, 2599-2610.

Ni, H., and Zhang, Y. (2008) H_2O diffusion models in rhyolitic melt with new high pressure data. Chemical Geology, 250, 68-78.

Ni, H., Shi, H., Zhang, L., Li, W.-C., Guo, X., and Liang, T. (2018) Cu diffusivity in granitic melts with application to the formation of porphyry Cu deposits. Contributions to Mineralogy and Petrology, 173, 50.

Ni, P., and Zhang, Y. (2016) Cu diffusion in a basaltic melt. American Mineralogist, 101, 1474-1482.

Ni, P., Zhang, Y., Simon, A., and Gagnon, J. (2017) Cu and Fe diffusion in rhyolitic melts during chalcocite "dissolution": implications for porphyry ore deposits and tektites. American Mineralogist, 102, 1287-1301.

O'Neill, H.S.C., Berry, A.J., and Eggins, S.M. (2008) The solubility and oxidation state of tungsten in silicate melts: implications for the comparative chemistry of W and Mo in planetary differentiation processes. Chemical Geology, 255, 346-359.

Ossandon, G.C., Freraut, R.C., Gustafson, L.B., Lindsay, D.D., and Zentilli, M. (2001) Geology of the Chuquicamata mine: a progress report. Economic Geology, 96, 249-270.

Richards, J.P. (2005) Cumulative factors in the generation of giant calc-alkaline porphyry Cu deposits. In Porter, T.M. (ed.) Super porphyry copper and gold deposits: A global perspective. PGC Publishing, Adelaide, South Australia, 1, 7–25.

Robb, L. (2004) Introduction to ore-forming processes, 373 p. Blackwell publishing,

Oxford.

Seedorff, E., Dilles, J.D., Proffett, J.M., Jr., Einaudi, M.T., Zurcher, L., Stavast, W.J.A., Johnson, D.A., and Barton, M.D. (2005) Porphyry deposits: characteristics and origin of hypogene features. Economic Geology 100th Anniversary Volume, 251-298.

Shannon, R.D. (1976). Revised effective ionic radii and systematic studies of interatomic distances in halides and chalcogenides. Acta crystallographica, A32, 751-767.

Sillitoe, R.H. (2010) Porphyry copper systems. Economic geology, 105, 3-41.

Simon, A.C., and Ripley, E.M. (2011) The role of magmatic sulfur in the formation of ore deposits. Reviews in Mineralogy and Geochemistry, 73, 513-578.

Singer, D.A. (1995) World class base and precious metal deposits; a quantitative analysis. Economic Geology, 90, 88-104.

Stoffell, B., Wilkinson, J.J., and Jeffries, T.E. (2004) Metal transport and deposition in hydrothermal veins revealed by 213 nm UV laser ablation microanalysis of single fluid inclusions. American Journal of Science, 304, 533-557.

Tattitch, B.C., and Blundy, J.D. (2017) Cu-Mo partitioning between felsic melts and saline-aqueous fluids as a function of X_{NaCleq}, f_{O2}, and f_{S2}. American Mineralogist, 102, 1987-2006.

Wade, J., Wood, B.J., and Norris, C.A. (2013) The oxidation state of tungsten in silicate melt at high pressures and temperatures. Chemical Geology, 335, 189-193.

508 Wilkinson, J.J. (2013) Triggers for the formation of porphyry ore deposits in magmatic
509 arcs. Nature Geoscience, 6, 917.
510 Withers, A.C., and Behrens, H. (1999) Temperature-induced changes in the NIR spectra
511 of hydrous albitic and rhyolitic glasses between 300 and 100 K. Physics and
512 Chemistry of Minerals, 27, 119-132.
513 Zajacz, Z., Halter, W. E., Pettke, T., and Guillong, M. (2008) Determination of fluid/melt
514 partition coefficients by LA-ICPMS analysis of co-existing fluid and silicate melt
515 inclusions: controls on element partitioning. Geochimica et Cosmochimica Acta,
516 72, 2169-2197.
517 Zhang, Y. (2008) Geochemical Kinetics, 656 p. Princeton University, Princeton.
518 Zhang, Y., Ni, H., and Chen, Y. (2010) Diffusion data in silicate melts. Reviews in
519 Mineralogy and Geochemistry, 72, 311-408.
520

FIGURE CAPTIONS

FIGURE 1. Sketches of samples in diffusion experiments: **(a)** diffusion couple composed of a Mo-rich, W-poor glass cylinder (with ~1900 ppm Mo and ~300 ppm W) and a W-rich, Mo-poor glass cylinder (with ~1900 ppm W and ~300 ppm Mo), sealed in a Pt capsule; **(b)** Mo saturation method involving an undoped glass cylinder and a Mo sheet serving as the source of Mo.

FIGURE 2. Photomicrograph of experimental products: **(a)** sample Anhy-Gran-2; the two halves coalesced after the experiment, but the interface distinguishes itself by tiny intrusion of Pt capsule walls; **(b)** sample Hydr-Gran-7 after Mo saturation experiment. For each sample, laser ablation pits along three profiles are indicated.

FIGURE 3. Diffusion profiles of Mo and W from four diffusion couple experiments. (**a)**, (**b)** and (**c)** anhydrous granitic melts; (**d)** hydrous granitic melt with 3.9 wt% H_2O, with three points of original concentrations (squares) added at the W-rich end due to damage of the sample during polishing. Solid circles denote data of the central profile, and open circles and crosses denote data from two side profiles. The curves are error function fits of the central profiles.

FIGURE 4. Diffusion profiles of Mo from nine Mo saturation experiments. (**a)** anhydrous granitic melt; (**b)**, **(c)** and (**d)** hydrous granitic melt with ~2.7 wt% H_2O; **(e)**, **(f)**, **(g) and (h)** hydrous granitic melt with ~5.1 wt% H_2O; **(i)** hydrous granitic melt with ~4.4 wt% H_2O (5.1 wt% dropped to 3.6 wt%). Solid circles denote data of the central profile, and open circles and crosses denote data from side profiles. A few odd points near the interface (marked in grey) are excluded from fitting. The curves are error function fits of the central profiles.

FIGURE 5. Variation of Mo concentration at the melt-Mo interface in Mo saturation experiments with temperature and H_2O content. Anomalous interface concentration is observed for Hydr-Gran-9 at 1000 °C in which H_2O content dropped from 5.1 wt% to 3.6 wt%. See text for detailed interpretation.

FIGURE 6. Arrhenius plot of the diffusivity data of Mo (solid symbols) and W (open symbols) in granitic melts at 1 GPa obtained in the present study. For Mo diffusivity in anhydrous melt, the data from diffusion couple experiments are shown in circles and a single datum from a Mo saturation experiment is shown in cross. The squares and triangles represent Mo diffusivities from Mo saturation experiments, and the diamonds represent Mo and W diffusivities from a diffusion couple experiment, with H_2O contents of melts marked in the labels. Error bars are smaller than the symbol sizes.

561

562 **FIGURE 7.** Variation of (**a)** Mo diffusivity at 1400 °C; (**b)** the pre-exponential factor D_0;
563 and (**c)** the activation energy for Mo diffusion in granitic melts with H_2O content. Error
564 bars are at 1σ level.

565

566 **FIGURE 8.** Comparison of diffusivities of Mo and W obtained in this study (solid lines)
567 with literature diffusivity data of W and other species (dashed lines and symbols) in
568 granitic melts. Water contents are given in the labels for hydrous melts. The triangles
569 denote W diffusivity data in Mungall et al. (1999) for both a granitic melt and that melt
570 with 20 wt% added Na_2O. Ca, Nb, Ta, Mungall et al. (1999); Cu, Ni et al. (2017); H_2O,
571 Ni and Zhang (2008).

572

573 **FIGURE 9.** Variation of enrichment factor of Mo and W (concentration in the fluid over
574 that in the melt) for a range of fluid-melt partition coefficients (K) and parameter γ
575 depends on the ratio of Mo or W diffusivity over water diffusivity in the melt. Calculated
576 with the trace element diffusion-partitioning model in Zhang (2008).

This is a preprint, the final version is subject to change, of the American Mineralogist (MSA)
Cite as Authors (Year) Title. American Mineralogist, in press.
DOI: https://doi.org/10.2138/am-2018-6569

TABLE 1. Chemical compositions of the synthesized granitic glasses in wt%

	Chuquicamata[a]	Starting material [b]			After experiment [c]			
		Anhy-Gran	Anhy-Gran-Mo	Anhy-Gran-W	Anhy-Gran-1	Hydr-Gran-1	Hydr-Gran-2	Hydr-Gran-5
SiO_2	69.83	70.96±0.48	71.08±0.44	70.39±0.27	70.07±0.32	70.06±0.29	70.92±0.99	70.37±0.48
TiO_2	0.27	0.23±0.03	0.25±0.04	0.18±0.06	0.29±0.01	0.29±0.01	0.28±0.02	0.29±0.01
Al_2O_3	16.54	15.59±0.15	15.44±0.31	15.96±0.28	16.31±0.18	16.42±0.16	16.42±0.64	16.15±0.28
FeO_t	1.67	1.64±0.11	1.74±0.09	1.68±0.13	1.61±0.21	1.37±0.04	0.87±0.06	1.00±0.07
MgO	0.58	0.56±0.03	0.60±0.04	0.53±0.03	0.55±0.01	0.60±0.01	0.59±0.05	0.60±0.01
CaO	1.74	1.36±0.06	1.38±0.06	1.38±0.03	1.69±0.04	1.72±0.03	1.67±0.15	1.69±0.05
Na_2O	4.04	3.80±0.09	3.82±0.12	3.88±0.08	3.97±0.06	3.98±0.05	3.86±0.13	3.91±0.05
K_2O	5.34	5.14±0.07	5.01±0.13	5.15±0.08	5.13±0.07	5.18±0.10	5.04±0.18	5.24±0.07
Total		99.28	99.24	99.15				
Mo			0.189±0.003	0.030±0.001				
W			0.030±0.001	0.199±0.004				
H_2O		0.01	0.01	0.01	0.04	3.92	2.70	5.11

[a] The target composition: East porphyry of the Chuquicamata complex, Chile (Ballard, 2001), normalized to 100%.

[b] Composition of initial anhydrous granitic glasses, with the major element contents from electron microprobe, Mo and W concentrations from LA-ICP-MS, and H_2O contents from FTIR. Standard deviations are at 1σ level.

[c] Composition of experimental products, with the major element contents from LA-ICP-MS (normalized to 100%) and H_2O contents from FTIR. Standard deviations are at 1σ level.

This is a preprint, the final version is subject to change, of the American Mineralogist (MSA)
Cite as Authors (Year) Title. American Mineralogist, in press.
DOI: https://doi.org/10.2138/am-2018-6569

TABLE 2. Summary of conditions and results of Mo and W diffusion experiments

Run No.	Type [a]	T (°C)	t (h)	D [c] (10^{-12} m^2/s)		H_2O (wt%)			C_0 [d] (ppm)
				Mo	W	initial	final	**mean**	
Anhy-Gran-1	Diff-cp	1600 ± 20	4	0.572 ± 0.010	0.536 ± 0.015	0.01	0.06	**0.04**	
Anhy-Gran-2	Diff-cp	1500 ± 20	22	0.119 ± 0.004	0.101 ± 0.004	0.01	0.19	**0.10**	
Anhy-Gran-3	Diff-cp	1400 ± 15	93	0.029 ± 0.001	0.026 ± 0.001	0.01	0.11	**0.06**	
Anhy-Gran-4	Mo-sat	1600 ± 20	4	0.65 ±0.01		0.01	0.10	**0.05**	3764 ± 18
Hydr-Gran-1	Diff-cp	1600 ± 20	1	8.79 ± 0.36	7.00 ± 0.34	3.93	3.91	**3.92**	
Hydr-Gran-2	Mo-sat	1600 ± 20	1	5.97 ± 0.13		2.83	2.56	**2.70**	7477 ± 69
Hydr-Gran-3	Mo-sat	1500 ± 20	3	2.47 ± 0.14		2.85	2.65	**2.75**	5570 ± 99
Hydr-Gran-4 [b]	Mo-sat	1400 ± 15	7	1.18 ± 0.05		3.02	2.32	**2.67**	5034 ± 72
Hydr-Gran-5	Mo-sat	1400 ± 15	1	8.99 ± 0.42		5.11	5.10	**5.11**	15134 ± 247
Hydr-Gran-6	Mo-sat	1300 ± 15	2	4.69 ± 0.19		5.11	5.05	**5.08**	7908 ± 127
Hydr-Gran-7	Mo-sat	1200 ± 15	3	3.40 ± 0.12		5.11	5.06	**5.09**	2785 ± 36
Hydr-Gran-8	Mo-sat	1100 ± 15	11	1.00 ± 0.05		5.10	4.78	**4.94**	2469 ± 62
Hydr-Gran-9 [b]	Mo-sat	1000 ± 15	43	0.052 ± 0.001		5.10	3.60	**4.35**	18206 ± 178

[a] "Diff-cp" and "Mo-sat" represent experiment approach of diffusion couple and Mo saturation, respectively.

[b] These two runs show notable water loss.

[c] Diffusivities (with errors at 1σ level) extracted from fitting diffusion couple or Mo saturation profiles.

[d] Mo concentrations (with errors at 1σ level) at the interface in Mo saturation experiments, obtained from fitting.

This is a preprint, the final version is subject to change, of the American Mineralogist (MSA)
Cite as Authors (Year) Title. American Mineralogist, in press.
DOI: https://doi.org/10.2138/am-2018-6569

Figure 1

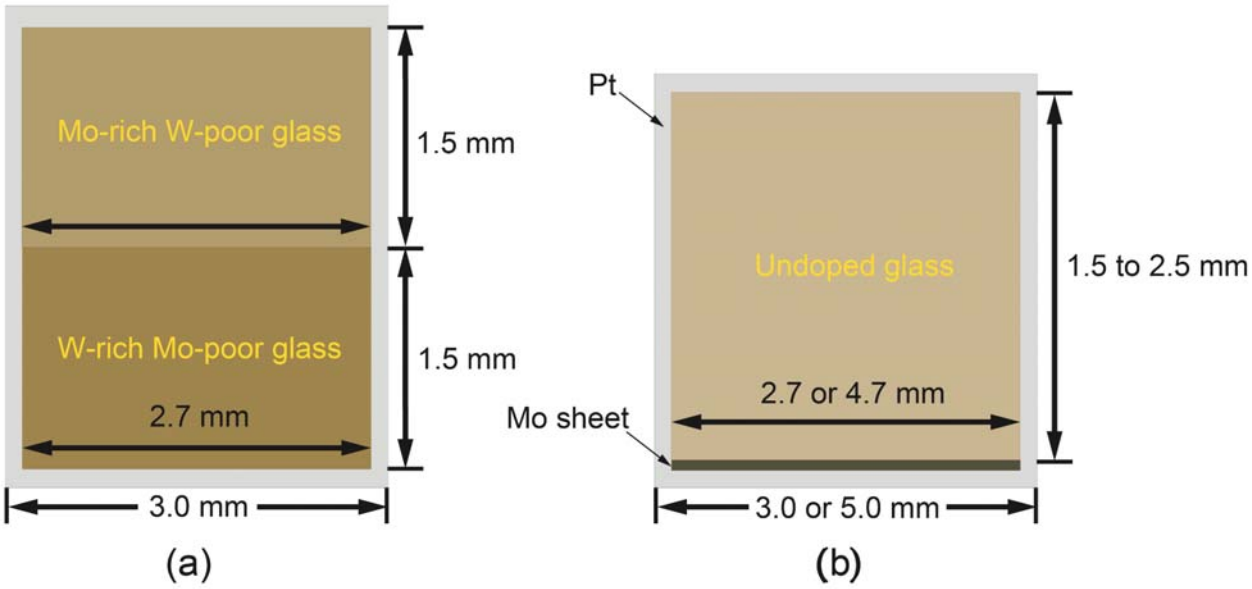

This is a preprint, the final version is subject to change, of the American Mineralogist (MSA)
Cite as Authors (Year) Title. American Mineralogist, in press.
DOI: https://doi.org/10.2138/am-2018-6569

Figure 2

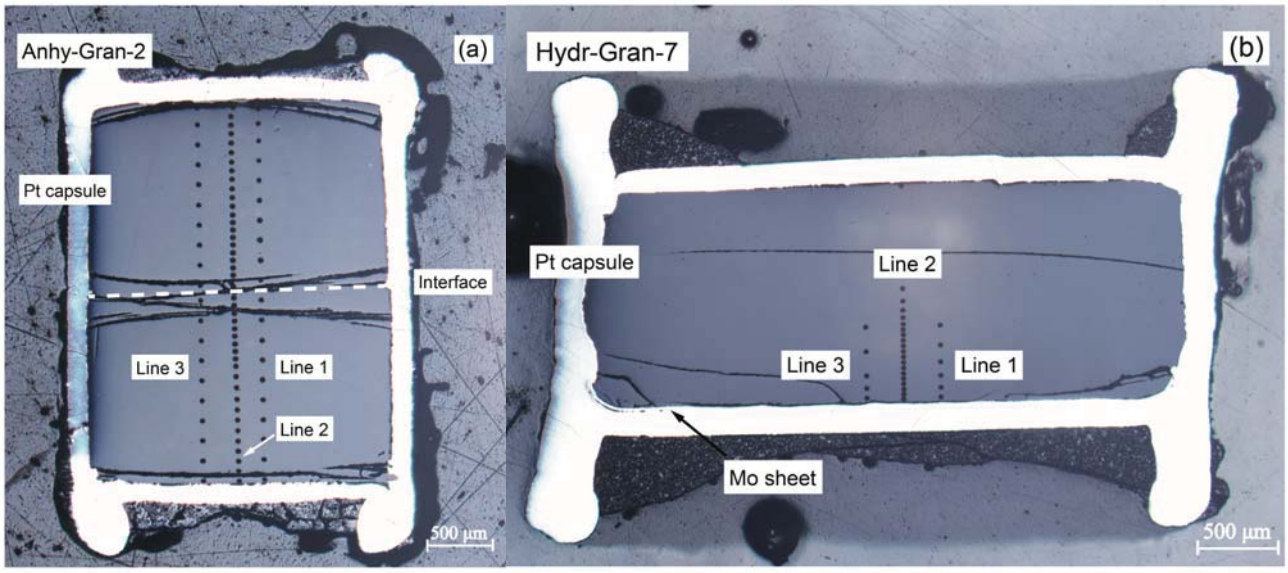

This is a preprint, the final version is subject to change, of the American Mineralogist (MSA)
Cite as Authors (Year) Title. American Mineralogist, in press.
DOI: https://doi.org/10.2138/am-2018-6569

Figure 3

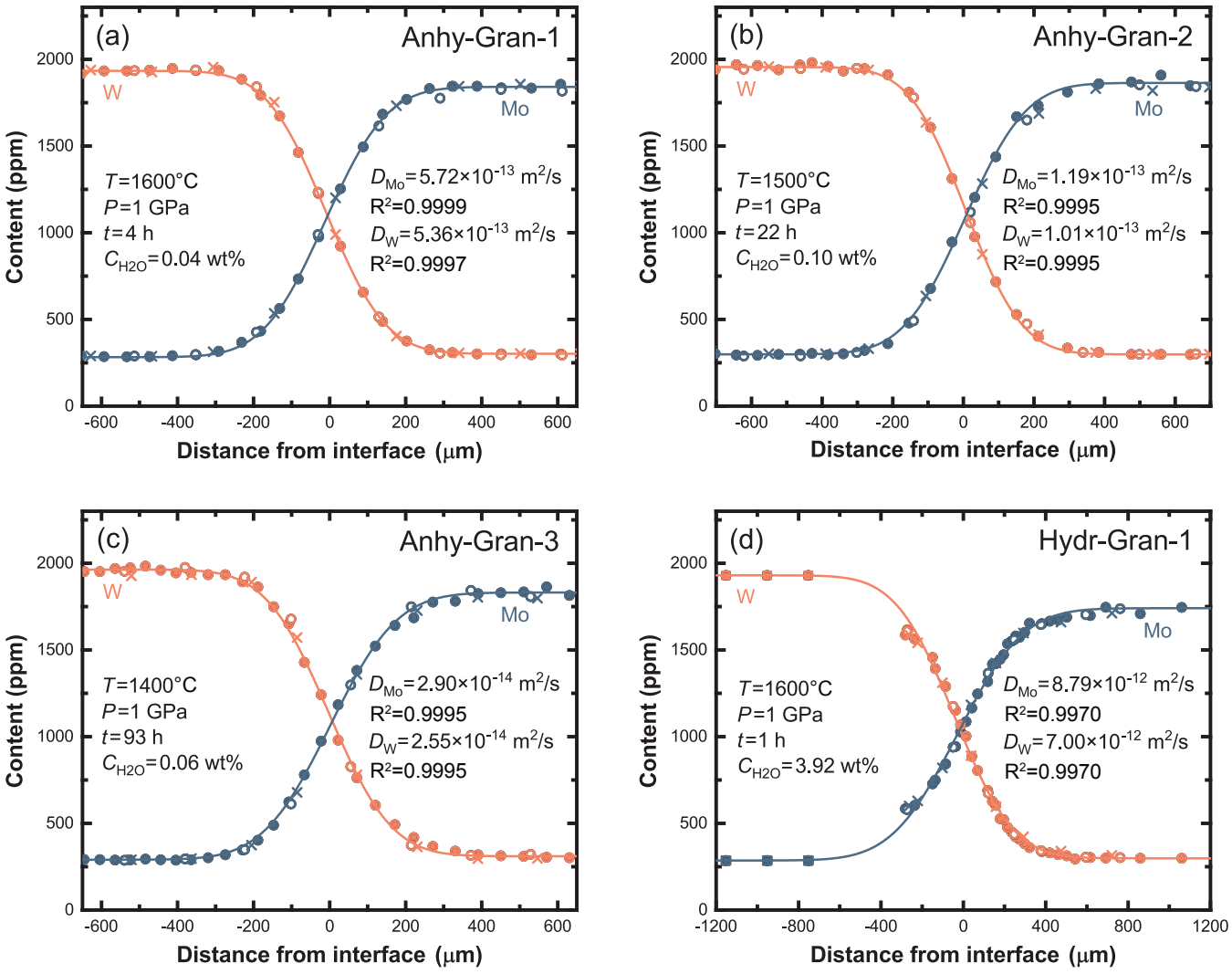

This is a preprint, the final version is subject to change, of the American Mineralogist (MSA)
Cite as Authors (Year) Title. American Mineralogist, in press.
DOI: https://doi.org/10.2138/am-2018-6569

Figure 4

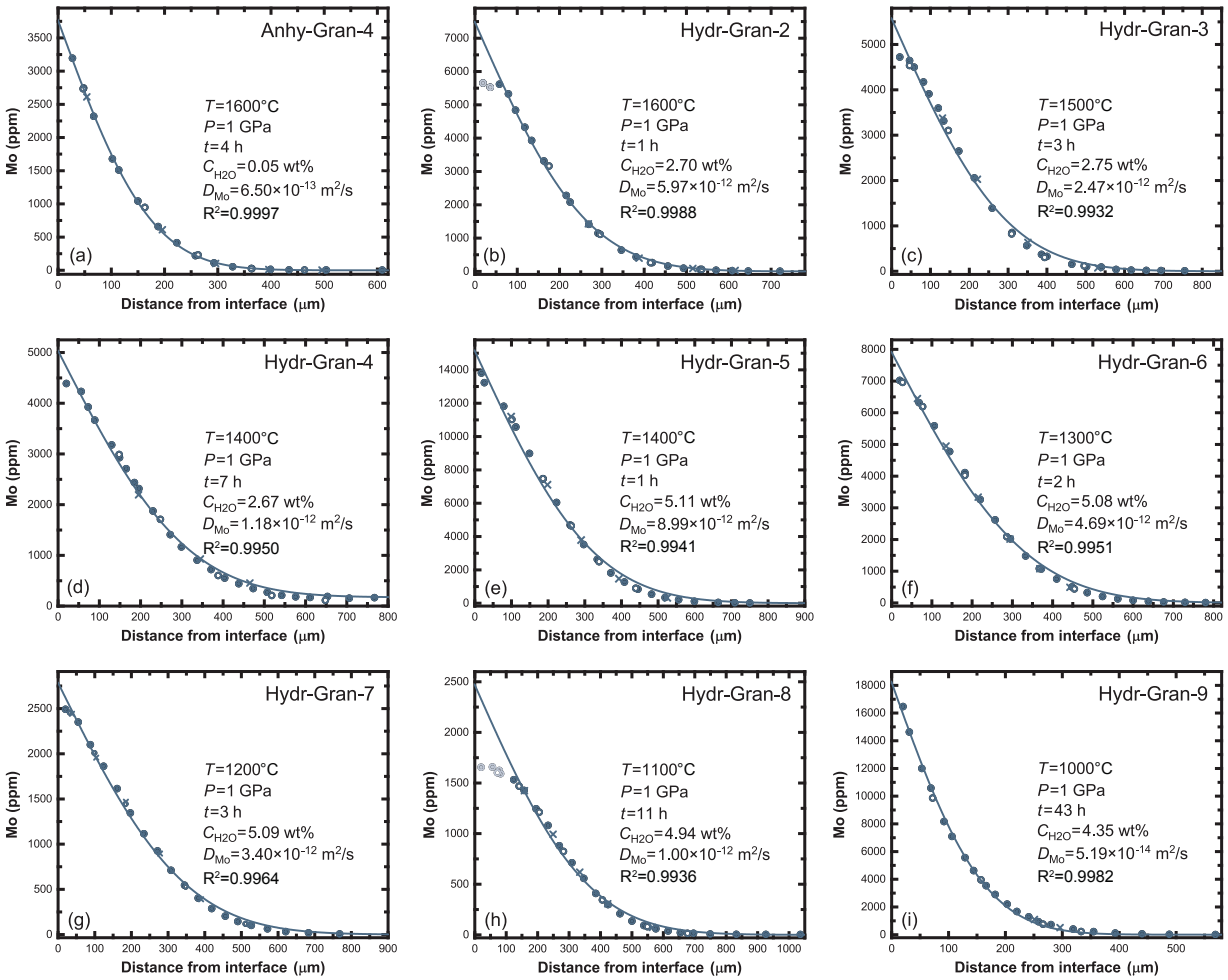

This is a preprint, the final version is subject to change, of the American Mineralogist (MSA)
Cite as Authors (Year) Title. American Mineralogist, in press.
DOI: https://doi.org/10.2138/am-2018-6569

Figure 5

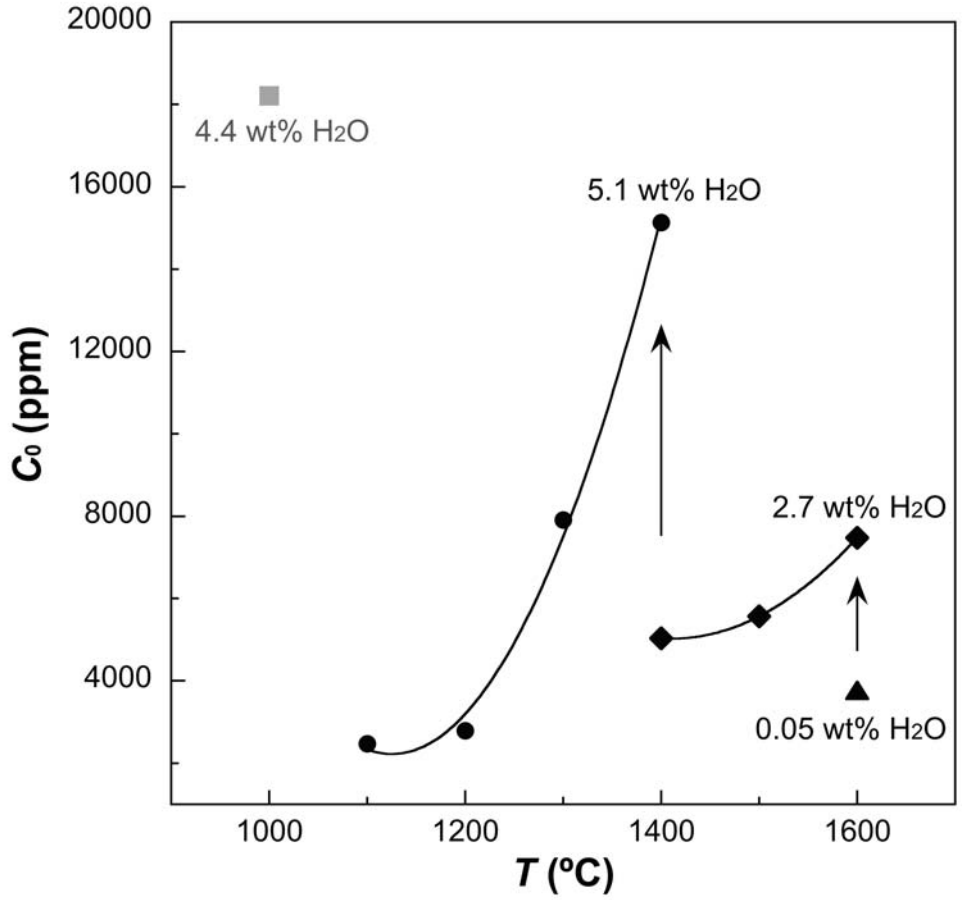

This is a preprint, the final version is subject to change, of the American Mineralogist (MSA)
Cite as Authors (Year) Title. American Mineralogist, in press.
DOI: https://doi.org/10.2138/am-2018-6569

Figure 6

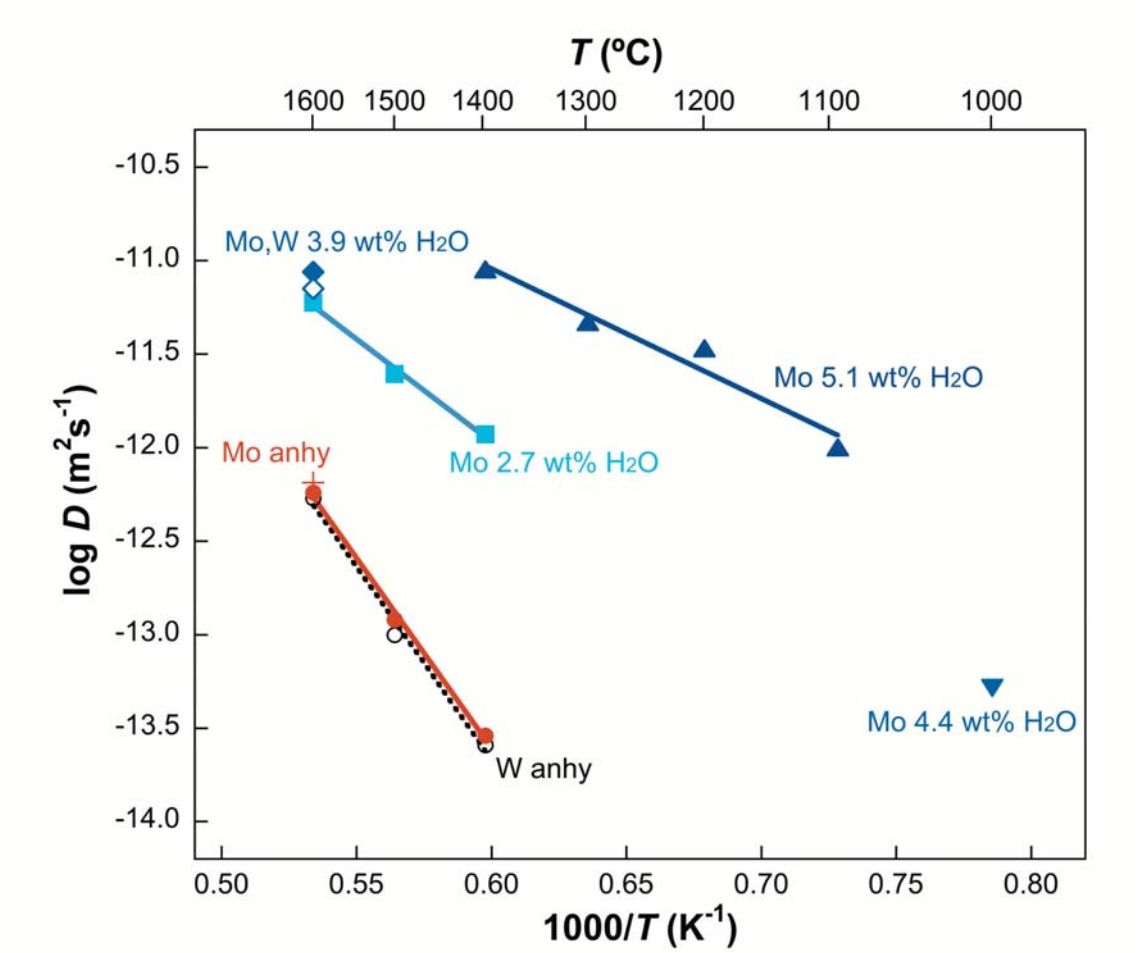

This is a preprint, the final version is subject to change, of the American Mineralogist (MSA)
Cite as Authors (Year) Title. American Mineralogist, in press.
DOI: https://doi.org/10.2138/am-2018-6569

Figure 7

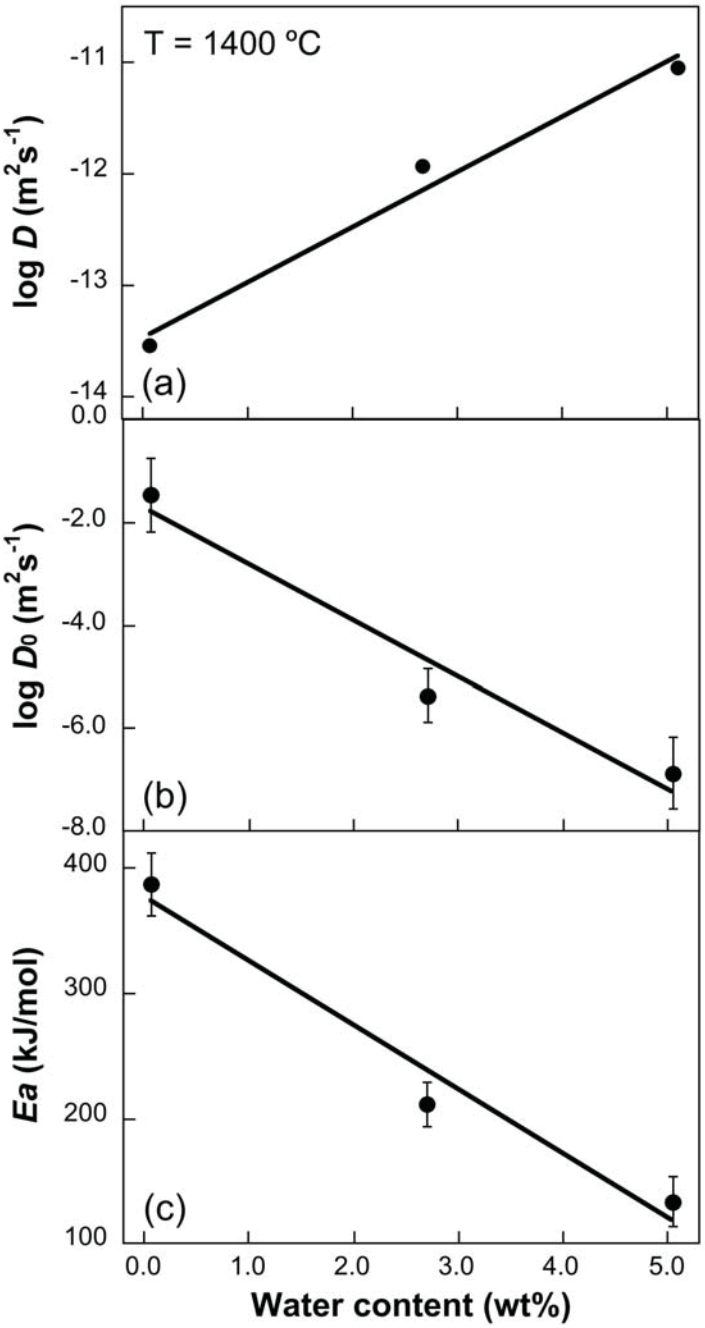

This is a preprint, the final version is subject to change, of the American Mineralogist (MSA)
Cite as Authors (Year) Title. American Mineralogist, in press.
DOI: https://doi.org/10.2138/am-2018-6569

Figure 8

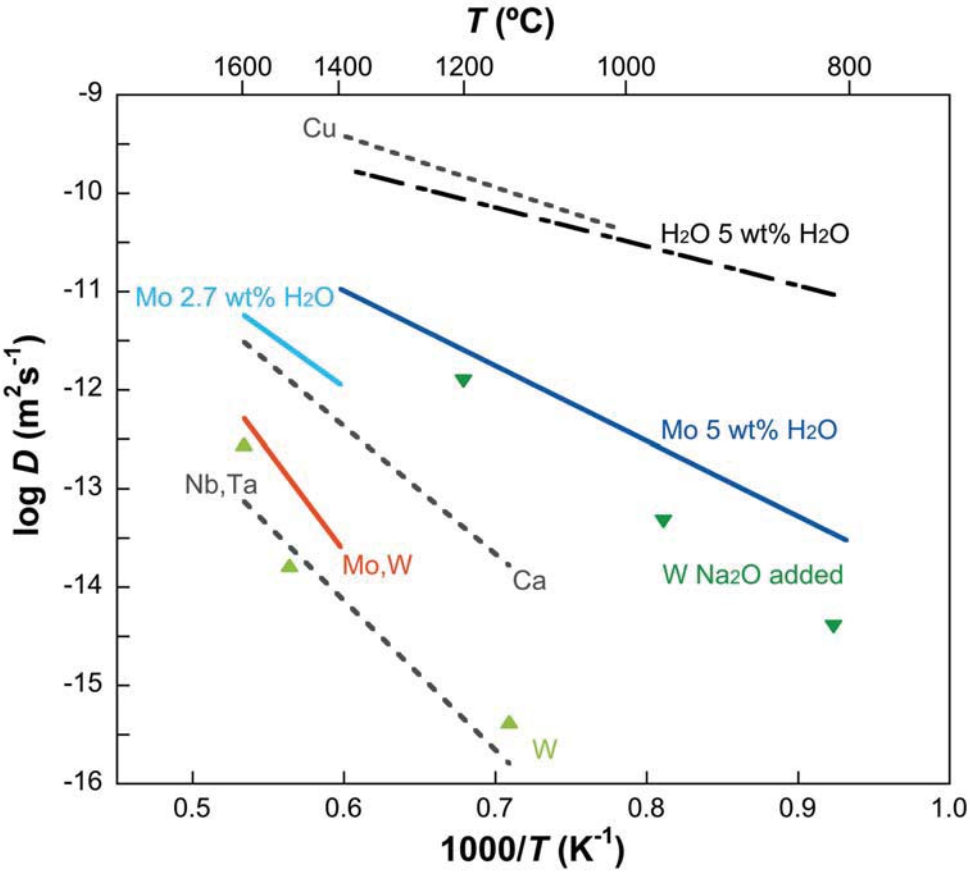

This is a preprint, the final version is subject to change, of the American Mineralogist (MSA)
Cite as Authors (Year) Title. American Mineralogist, in press.
DOI: https://doi.org/10.2138/am-2018-6569

Figure 9